



NIH PUBLIC ACCESS

Author Manuscript

Ophthalmology. Author manuscript; available in PMC 2015 July 01.

Published in final edited form as:

Ophthalmology. 2014 July ; 121(7): 1435–1444. doi:10.1016/j.ophtha.2014.01.034.

Quantitative optical coherence tomography angiography of choroidal neovascularization in age-related macular degeneration

Yali Jia, PhD^{1,*}, Steven T. Bailey, MD^{1,*}, David J. Wilson, MD¹, Ou Tan, PhD¹, Michael L. Klein, MD¹, Christina J. Flaxel, MD¹, Benjamin Potsaid, PhD^{2,3}, Jonathan J. Liu, MS², Chen D. Lu, MS², Martin F. Kraus, MS^{2,4}, James G. Fujimoto, PhD², and David Huang, MD, PhD¹

¹Casey Eye Institute, Oregon Health and Science University, Portland, Oregon, USA

²Department of Electrical Engineering & Computer Science, Massachusetts Institute of Technology, Cambridge, Massachusetts, USA

³Advanced Imaging Group, Thorlabs, Inc., Newton, New Jersey, USA

⁴Pattern Recognition Lab and School of Advanced Optical Technologies (SAOT), University Erlangen-Nuremberg, D-91058 Erlangen, Germany

Abstract

Purpose—To detect and quantify choroidal neovascularization (CNV) in age-related macular degeneration (AMD) patients using optical coherence tomography (OCT) angiography.

Design—Observational, cross-sectional study.

Participants—Five normal subjects and five neovascular AMD patients were included.

Methods—Five eyes with neovascular AMD and five normal age-matched controls were scanned by a high-speed (100,000 A-scans/sec) 1050 nm wavelength swept-source OCT. The macular angiography scan covered a 3×3 mm area and comprised 200×200×8 A-scans acquired in 3.5 sec. Flow was detected using the split-spectrum amplitude-decorrelation angiography (SSADA) algorithm. Motion artifacts were removed by three dimensional (3D) orthogonal registration and merging of 4 scans. The 3D angiography was segmented into 3 layers: inner retina

© 2014 American Academy of Ophthalmology, Inc. Published by Elsevier Inc. All rights reserved.

Correspondence: David Huang, MD, PhD, davidhuang@alum.mit.edu, Weeks Professor of Ophthalmic Research, Casey Eye Institute, Oregon Health & Science University, 3375 SW Terwilliger Blvd. Portland, OR 97239-4197, USA; Phone (503) 494-0633.

*These authors contributed equally to this work

Disclosure

Oregon Health & Science University (OHSU), Yali Jia, Ou Tan and David Huang have a significant financial interest in Optovue, Inc., a company that may have a commercial interest in the results of this research and technology. These potential conflicts of interest have been reviewed and managed by OHSU. James G. Fujimoto and David Huang receive royalties on an optical coherence tomography patent licensed by the Massachusetts Institute of Technology (MIT) to Carl Zeiss Meditec and LightLab Imaging. James G. Fujimoto, Benjamin Potsaid and Martin F. Kraus receive royalties from intellectual property owned by MIT and licensed to Optovue, Inc. Other authors do not have financial interest in the subject of this article.

Publisher's Disclaimer: This is a PDF file of an unedited manuscript that has been accepted for publication. As a service to our customers we are providing this early version of the manuscript. The manuscript will undergo copyediting, typesetting, and review of the resulting proof before it is published in its final citable form. Please note that during the production process errors may be discovered which could affect the content, and all legal disclaimers that apply to the journal pertain.

(to show retinal vasculature), outer retina (to identify CNV), and choroid. *En face* maximum projection was used to obtain 2D angiograms from the 3 layers. CNV area and flow index were computed from the *en face* OCT angiogram of the outer retinal layer. Flow (decorrelation) and structural data were combined in composite color angiograms for both *en face* and cross-sectional views.

Main Outcome Measurements—CNV angiogram, CNV area, and CNV flow index.

Results—*En face* OCT angiograms of CNVs showed sizes and locations that were confirmed by fluorescein angiography. OCT angiography provided more distinct vascular network patterns that were less obscured by subretinal hemorrhage. The *en face* angiograms also showed areas of reduced choroidal flow adjacent to the CNV in all cases and significantly reduced retinal flow in one case. Cross-sectional angiograms were used to visualize CNV location relative to the retinal pigment epithelium and Bruch's layer and classify type I and type II CNV. A feeder vessel could be identified in one case. Higher flow indexes were associated with larger CNV and type II CNV.

Conclusions—OCT angiography provides depth-resolved information and detailed images of CNV in neovascular AMD. Quantitative information regarding CNV flow and area can be obtained. Further studies are needed to assess the role of quantitative OCT angiography in the evaluation and treatment of neovascular AMD.

Age-related macular degeneration (AMD) is the leading cause of blindness in older adults of European descent.¹ Neovascular AMD is an advanced form of macular degeneration that historically has accounted for the majority of vision loss related to AMD.² It is characterized by the presence of choroidal neovascularization (CNV) consisting of abnormal blood vessels that originate from the choroid. The vessels grow through Bruch's membrane (BM) and extend into the subretinal pigment epithelial (RPE) and/or subretinal space. CNV can result in hemorrhage, fluid exudation, and fibrosis, resulting in photoreceptor damage and vision loss.³ To diagnose neovascular AMD and evaluate the efficacy of treatment, determination of the presence and precise location of the CNV lesion is essential.

Fluorescein angiography (FA) and indocyanine-green angiography (ICGA) are important diagnostic tools used to detect and evaluate CNV in clinical practice. Leakage of dye in the later frames of the angiogram is used to identify the presence of the CNV. Both FA and ICGA require intravenous dye injection, which can result in nausea and, rarely, anaphylaxis.^{4, 5}

Optical coherence tomography (OCT) generates cross-sectional images by measuring the echo time delay and magnitude of backscattered light.⁶ OCT has achieved micrometer-level axial resolution in cross-sectional retinal imaging. The earliest retinal OCT imaging for studying neovascular AMD was based on first-generation time-domain OCT technology, which has limited speed and sensitivity.⁷⁻⁹ Spectral-domain OCT has greatly improved speed and sensitivity and is able to detect small changes in the morphology of the retinal layers and CNV activity in neovascular AMD.^{10, 11} More recently, swept-source OCT has demonstrated improved ranging depth by using a rapidly tuned laser and a longer wavelength (1050-nm spectral range) allowing for improved imaging beneath the RPE.¹² Therefore, this novel OCT modality is under study and may allow for better visualization of the CNV beneath the RPE.

Structural OCT, using any technology, is only sensitive to backscattering light intensity and cannot detect blood flow information. Due to this limitation, structural OCT cannot reliably discriminate vascular tissue from the surrounding tissues; hence, the precise location and activity of the CNV cannot be determined. Since 2007, several phase-based (e.g. Doppler shift,^{13, 14} Doppler variance,^{15–17} and phase-variance^{18, 19}) and intensity-based (e.g. speckle variance^{20–22} and decorrelation^{23, 24}) OCT angiography methods have been described for three dimensional (3D) noninvasive vasculature mapping at the microcirculation level. Miura et al²⁵ and Hong et al²⁶ recently demonstrated Doppler optical coherence angiography for imaging 3D views of ocular vascular pathology in polypoidal choroidal vasculopathy and exudative macular diseases, respectively.

Recently our group has developed the split-spectrum amplitude-decorrelation angiography (SSADA) algorithm to improve signal-to-noise ratio of flow detection. This technique enables OCT angiography within a practical image acquisition time (few seconds) using a prototype that is only slightly faster than the newest generation of commercial systems. We have performed the first clinical study for demonstrating ocular vascular disturbances in glaucoma.²⁷

In this study, we used OCT angiography with the SSADA algorithm²³ to investigate CNV associated with neovascular AMD. A descriptive case series of neovascular AMD is presented to describe the usefulness of OCT angiography for visualizing 3D vascular architecture and quantifying the blood flow within CNV.

METHODS

Study population

Patients were selected from clinical retina practices at the Casey Eye Institute. Patients diagnosed with neovascular AMD underwent a comprehensive eye exam and routine diagnostic evaluation consisting of color fundus photography, FA, and OCT (Spectralis; Heidelberg Engineering, Heidelberg, Germany). Inclusion criteria were patients over the age of 50 with the presence of drusen and treatment naïve CNV confirmed by fluorescein dye leakage on angiogram and presence of one of the following on OCT: subretinal fluid, intraretinal fluid, or subretinal pigment epithelial fluid. Exclusion criteria included subretinal hemorrhage greater than 50% of the CNV lesion, visual acuity less than 20/200, and media opacity interfering with OCT image quality, such as cataract.

OCT angiograms of normal subjects (aged 40 to 79) from a separate study, the “Functional and Structural Optical Coherence Tomography for Glaucoma” study, were used as controls in this study. Inclusion criteria from that study included: vision better than 20/40, no ocular surgery other than previous cataract surgery, and no eye disease affecting vision. As described below, 24 normal control subject’s images were used for normative retinal thickness measurements and five control subjects (age > 60) underwent OCT angiography processing.

Patients were enrolled after informed consent in accordance with an Institutional Review Board (IRB)/Ethics Committee approved protocol at Oregon Health & Science University

and in compliance with the Declaration of Helsinki. Once consent was obtained, patients underwent scanning with the prototype OCT system.

OCT angiography

The prototype high speed swept-source OCT system was built by the Laser Medicine and Medical Imaging Group at the Massachusetts Institute of Technology and followed the configuration published by Potsaid *et al.*²³ The device operated at an axial scan speed of 100 kHz using a swept source cavity laser operating at 1050 nm with a tuning range of 100 nm. A resolution of 5.3 μm axially and 18 μm laterally at an imaging depth of 2.9 mm in tissue was achieved. The ocular light power exposure was 1.9 mW, which was within the American National Standards Institute (ANSI) safety limit.²⁸

A 3 \times 3-mm scanning area centered on the fovea was captured for blood flow measurements. In the fast transverse scanning direction, 200 axial scans were sampled along a 3-mm region to obtain a single B-scan. Eight consecutive B-scans (M-B frames) were captured at a fixed position before proceeding to the next sampling location. A total of 200 locations along a 3-mm region in the slow transverse direction were sampled to form a 3-D data cube. With a B-scan frame rate of 455 frames per second, the 1,600 B-scans in each scan were acquired in approximately 3.5 seconds. Four volumetric raster scans, including two horizontal priority fast transverse (x-fast) scans and two vertical priority fast transverse (y-fast) scans, were obtained consecutively in one session.

The SSADA algorithm was used to distinguish blood flow from static tissue as described in detail in previous published paper and is briefly reviewed below. As seen in real-time OCT structural images, the amplitude of the signal returning from nonstatic tissue varies rapidly over time.²⁹ By calculating the decorrelation of signal amplitude from consecutive B-scans, a contrast between static and nonstatic tissue is created that allows for the visualization of blood flow. However, decorrelation can also be generated by bulk (non-flow) eye motion. The SSADA algorithm was developed to minimize bulk axial motion noise due to orbital pulsation by splitting the spectrum and thereby lengthening the axial resolution element. Additionally, the algorithm incorporated three steps to further remove motion artifact within each angiography scan. First, using outlier analysis, the decorrelation frames with excessive median decorrelation values (i.e., frames corrupted by saccadic and micro-saccadic eye movements) were removed at each M-B scan position and the remaining individual frames were averaged to obtain the final average decorrelation flow image. Second, if the number of remaining individual frames is less than three for averaging, the average decorrelation image at this location is replaced by the spatial neighbors. Third, the median decorrelation (an estimate of bulk motion effect) was calculated for each average decorrelation frame and then subtracted from it. This sets the decorrelation value for bulk tissue to around zero.

Physical flow phantom calibration experiments have been performed in our research group³⁰ and by others.³¹ Decorrelation can be considered as a metric for measuring fluctuation in the backscattered OCT signal amplitude (intensity) that does not depend on the average signal level. To be specific, the blood flow results in fluctuation in the amplitude of OCT fringes (speckle) as red blood cells move within a particular voxel. Hence the eight M-B frames contain fluctuating values of OCT output intensities at any given voxel in the flow of blood,

and the definition of decorrelation is constructed so that fluctuating intensities yield high decorrelation values (approaching 1.0). Pixels in the M-B frames that represent static tissue have constant intensities, and thus yield small decorrelation values (approaching 0). The faster blood particles move across the laser beam, the higher is the decorrelation of the received signals within a velocity range set by the scan parameters. In the other words, decorrelation is approximately linear to flow velocity (the distance traveled by red blood cells flowing across the light beam within a unit time).^{30, 31} However, beyond a saturation velocity that is defined by the time interval between consecutive OCT M-B frames, the decorrelation increases more slowly with velocity and eventually reaches an upper boundary.³¹ This saturation velocity should be approximately 0.3 to 0.7 mm/sec according to our³⁰ and others' physical phantom experiments,³¹ accounting for our wavelength of 1050 nm and inter-MB frame interval of 2 msec. The minimum velocity is approximately 0.02 mm/sec according to our phantom calibration. This is determined by the threshold decorrelation value 0.09, which is two standard deviations above the mean decorrelation value in the noise region, the central foveal avascular zone in normal eyes.

Motion artifacts were further corrected by applying an image registration algorithm that registered 4 orthogonal raster scanned volumes.³² Motion correction was first performed on the structural OCT data. The motion correction algorithm generated 3D displacement fields that map A-scans from the input volumes into a common motion-corrected space. The same displacement fields were applied to the decorrelation (flow) data to produce motion-corrected flow data volumes. Flow data from 4 input volumes were weighted and merged,³² improving the signal-to-noise ratio in the flow signal, and reducing the flow measurement variation due to local flow changes caused by the cardiac cycle.

To enhance visualization, the 3D angiogram was separately projected into *en face* views (Fig. 1, available at www.aaojournal.org) in 3 layers using an automated algorithm.^{33, 34} The inner retinal layer was defined from the internal limiting membrane (ILM) to the outer boundary of the outer plexiform layer (OPL). Thus defined, the inner retina should contain all of the normal retinal vasculature. The outer retinal layer was defined from the outer OPL to the BM. Since the outer retina is normally avascular, any flow in this layer could be interpreted as CNV. The choroidal layer was defined as below BM. All these boundaries were identified through the analysis of the reflectance and reflectance-gradient profiles in depth. Clinician's interpretation and manual identification of BM and the OPL was necessary when pathologies such as pigment epithelial detachment (PED) and intraretinal fluid obscured the outer retinal landmarks (AMD case # 3). Separate *en face* images of the inner retina, outer retina, and choroid were presented in a sepia color scale. A composite view was also developed, where each layer was assigned a different color (Figs. 1–4; Figs 1 and 4 available at www.aaojournal.org) to aid with visualization as follows. The inner retina contained normal retinal circulation and was coded purple. The outer retinal layer contained any potential CNV and was coded yellow. The choroid layer was coded red.

Structural OCT features were added to OCT angiography with composite *en face* view and color coding demonstrating subretinal fluid (dark blue) and intraretinal cysts (light blue). These two types of fluid are both detected using a level-set segmentation method³⁵ due to the fact that the reflectance of cysts and sub-retinal fluid is significantly lower than the

surrounding tissue in retina. Based on the difference between their position, shape, and size, these fluid regions can be classified as the intraretinal or the subretinal. Additionally, the variation in retinal thickness was calculated, normalized by the normal retina thickness range, and presented as a retinal thickness deviation map. For the purpose of this pilot study, an estimate of normal retinal thickness with the prototype OCT was obtained from 24 normal eyes from 24 subjects.

A method was also developed to remove flow projection artifacts. The cross-sectional angiogram (Fig. 1B, available at www.aaojournal.org) showed flow projection artifacts on the photoreceptor inner segment/outer segment (IS/OS) boundary and RPE. The projection artifacts were due to fluctuating shadows cast by flowing blood in large inner retinal vessels that cause variation in the reflected signal in deeper layers. The signal variation was detected as a decorrelation and could not be differentiated from true flow on its own. However, these artifacts were removed from under the flow pixels in the inner retina. To remove flow projection artifacts from superficial retinal blood vessels to outer retina, we first generated a binary large inner retinal vessel map by applying a 30×30 pixel Gaussian filter. This filter removed small inner retinal vessels and masked the outer retina flow map, thus enabling the subtraction of large vessel projections. A binary outer retinal flow map was then generated by applying a 10×10 pixel Gaussian filter to remove remaining noise and mask the outer retinal flow map again to obtain a clean map. After these artifacts were removed by the mask subtraction operation, there were no longer any flow artifacts in the normally avascular outer retina, as shown in the cross-sectional color angiogram (Fig. 1C) and the *en face* angiogram of the outer retina (Fig. 1E).

To quantify the blood flow within the CNV, the CNV area and flow index were calculated from the 2D maximum projection outer retina CNV angiogram. The CNV area was calculated by multiplying the number of pixels (for which the decorrelation value was above that of the background) and the pixel size. The CNV flow index was the average decorrelation value in the CNV region, given by,

$$\frac{\int_A D \cdot V dA}{\int_A dA} \quad (V=1, \text{ if vessel}; V=0, \text{ if not})$$

where D is the decorrelation value acquired by SSADA. V is 1 when decorrelation value was above background; otherwise, V is 0. Flow index is a dimensionless parameter between 0 and 1 that is proportional to the density of blood vessels (fractional area occupied by vessels) and the velocity of blood flow in the CNV region.

RESULTS

OCT angiograms of five neovascular AMD eyes were compared with five normal eyes. The CNV area and flow index was calculated from all neovascular AMD cases. None of the five normal cases had flow detected in outer retina and CNV area and flow index were zero. A representative normal control case and three of the neovascular AMD cases are presented.

Normal control case

A 69-year old female with no ocular disease served as a control case (Fig. 1, available at www.aaojournal.org). The inner retinal angiogram (Fig. 1D) showed the normal retinal circulation with a small foveal avascular zone of approximately 0.6 mm in diameter. The absence of any flow in the outer retinal layer (Fig. 1E) allowed easy detection of CNV in the cases to be shown later. The absence of blood flow in the outer retina was noted in all 5 normal control participants. The flow in the inner choroid was nearly confluent (Fig. 1C, 1F) and masked the vascular patterns in the outer choroid and sclera in the *en face* angiogram (Fig. 1F). The signal voids in the larger vessels in the outer choroid were due to the high flow velocity (Fig. 1A–C).

AMD case 1

A 65-year-old female noted vision loss in her right eye for one month. Visual acuity measured 20/100 in the right eye. Fundus photography (Fig. 2A) showed drusen and a small subretinal hemorrhage associated with a gray subretinal lesion just nasal to the fovea. FA (Fig. 2B, C) revealed early hyperfluorescence with late leakage consistent with classic CNV.

OCT angiography showed a normal retinal circulation (Fig. 2D, H). The outer retinal OCT angiogram (Fig. 2E, H) showed high flow in a CNV network in a pattern strikingly similar to the early phase of FA. The cross-sectional color OCT angiogram (Fig. 2G) showed the CNV to be underneath the RPE and above BM, indicating type I CNV. The subretinal hemorrhage above the CNV (Fig. 2G) did not seem to obscure the CNV on either the FA or OCT angiograms (Fig. 2E, H).

The *en face* OCT angiogram of the choroid (Fig. 2F) showed loss of choriocapillaris revealing deeper, larger choroidal vessels (compare to normal choroid in Fig. 1F). An area inferotemporal to the CNV had particularly low flow in both the choriocapillaris and deeper choroid (Fig. 2F, green outline). This low flow choroidal region had high OCT reflectance signal (Fig. 2G, green arrow), therefore the reduced flow was not caused by a shadow artifact.

The composite *en face* OCT angiogram (Fig. 2H) showed that the CNV was at the superonasal edge of the fovea avascular zone (FAZ) and that subretinal fluid was accumulated next to the CNV. The OCT retinal thickness map (Fig. 2I) showed retinal thickening over the CNV that was primarily due to the inclusion of subretinal hemorrhage (Fig. 2G) in the retinal thickness measurement, and an element of retinal edema inferior to the CNV. These *en face* OCT views combined angiographic (CNV size, location, flow) and structural information (fluid, edema) that would be useful for clinical management.

AMD case 2

A 76-year-old female noticed vision loss in her left eye for one week. Visual acuity measured 20/30, and fundus examination (Fig. 3A) of the left eye revealed drusen and a gray/green lesion in the temporal macula with associated subretinal hemorrhage. Early frames of the FA revealed a hyperfluorescent vascular network in the temporal macula with late leakage (Fig. 3B, C).

OCT angiography showed details of the CNV structure, with a central feeder vessel from which radiated thick core vessels ending in fine vascular fronds (Fig. 3E, J; Video 1, available at www.aaojournal.org). Both the FA and OCT angiogram show an identical CNV location, with slight notching at the superonasal edge due to shadowing from the small patch of subretinal hemorrhage. Cross-sectional OCT angiography (Figs. 3 G, H; Video 2, available at www.aaojournal.org) revealed that most of the CNV flow was above the RPE, indicating a predominantly type II CNV. Due to the flow projection artifact, there appeared to be flow in the RPE below the CNV.

The *en face* OCT angiogram of the choroid (Fig. 3F) showed patchy loss of choriocapillaris, which allowed visualization of intermediate-to-large deeper choroidal vessels that were not visible in the healthy control (Fig. 1F). There were focal regions under and adjacent to the CNV where there was greatly reduced flow in both the choriocapillaris and deeper choroid (Fig. 3F–H). Although some of this might be explained by shadowing under the CNV, the hypoperfused choroid adjacent to the CNV had normal OCT reflectance (Fig. 3I), suggesting that the loss of choroidal flow was real rather than an artifact.

The composite *en face* OCT angiogram showed that the CNV was at the superotemporal edge of the FAZ. Subretinal fluid accumulated superonasal to the CNV, and intraretinal cystic fluid accumulated above the CNV. Retinal thickening shown on the relative thickness map (Fig. 3K) correlated with the intraretinal fluid accumulation.

AMD case 3

An 88-year-old female noted vision loss in her right eye for several months (Fig. 4, available at www.aaojournal.org). Visual acuity in the right eye was 20/200. Fundus photography (Fig. 4A) demonstrated chronic geographic atrophy in the superior nasal macula with new subretinal hemorrhage and an associated RPE tear temporal to the geographic atrophy. Fluorescein angiography showed late leakage consistent with a CNV (Fig. 4B, C). However, the location of the CNV was unclear due to blocking from the subretinal hemorrhage. Hypofluorescence from the scrolled RPE and hyperfluorescence-associated geographic atrophy were evident.

The inner retinal angiogram in this case (Fig. 4D) showed an apparent reduction in inner retinal blood flow that may have indicated retinal atrophy. This patient had difficulty with fixation and slight motion artifacts (horizontal and vertical dark lines) were evident despite the use of 3D registration software.

OCT angiography of the outer retina (Fig. 4E–H) showed a distinct CNV adjacent to the subretinal hemorrhage. The nasal edge of the CNV was blocked from view where the subretinal hemorrhage was thicker and cast a shadow. The cross-sectional OCT angiogram (Fig. 4G) revealed high CNV flow at the edge of the RPE tear. Flow was detected both above and below the RPE, indicating a combined type I and type II lesion. Besides the CNV, there was also accumulation of a large amount of stationary (nonvascular) material under the PED.

The *en face* choroidal angiogram (Fig. 4F) showed reduced signal both under the PED and in the area of geographic atrophy. The area under the PED showed low reflectance on OCT cross-section (Fig. 4G) and no vascular pattern on the *en face* OCT angiogram (Fig. 4F). This suggested that the reduced choroidal flow was a shadow artifact associated with the PED and scrolled RPE (Fig. 4F). A similar area of blocked fluorescence was present on FA (Fig. 4B, C). In contrast, the area of geographic atrophy showed distinct large, deep choroidal vessels and loss of choriocapillaris.

The composite *en face* OCT angiogram (Fig. 4H) showed the CNV to be inferior to the FAZ and associated with a surrounding accumulation of both intraretinal and subretinal fluids. There was retinal thinning over the CNV (Fig. 4I), possibly due to focal compression from the highly elevated CNV and RPE tear (Fig. 4G). There was gross retinal thickening around the CNV (Fig. 4I) associated with fluid accumulation (Fig. 4H). The heavy accumulation of intraretinal fluid and reduced retinal blood flow visualized on the *en face* composite OCT angiogram may explain the poor visual acuity.

Evaluation of choroidal flow in AMD

OCT angiography of the choroid showed reduced inner choroidal flow in all five AMD cases compared to the control cases that allowed visualization of larger and deeper choroidal vessels. Conventional FA and structural OCT did not reveal geographic atrophy or other abnormalities that accounted for the choriocapillaris atrophy in most of these areas. In addition, focal areas of decreased flow in both superficial and deeper choroidal vessels were associated with CNV in all of the AMD cases, except for Case 3, where the presence of a focal choroidal flow defect could not be determined because of shadowing by the scrolled RPE (Fig. 4F).

Quantification of the area and flow index of CNV

Quantitative measurements of CNV area and flow index were summarized in Table 1. High flow index indicated active blood flow within the CNV. Higher flow was detected with larger CNVs and those that were type II compared to type I and combined CNVs.

DISCUSSION

Structural OCT has become an indispensable tool in the management of AMD. It allows the clinician to assess fluid exudation from CNV as manifested by intraretinal cysts, retinal thickening, and subretinal fluid accumulation. It identifies the alterations in normal retinal anatomy that are associated with visual potential. However, structural OCT images cannot identify the CNV structure itself. Although structural OCT can identify abnormal tissue above or below the RPE that might be CNV, positive identification is not possible because CNV tissue has similar reflectivity as drusenoid material, hemorrhage, RPE, and choroid.³⁶ Therefore FA or ICGA are still needed in the initial diagnosis of neovascular AMD. Because FA and ICGA require intravenous dye injection, nausea and vomiting are common adverse reactions, and serious anaphylactic reactions are possible.^{4, 5} Therefore it is highly desirable to develop a noninvasive method of imaging CNV. Unfortunately, 2D flow imaging technologies such as scanning laser Doppler flowmetry,³⁷ laser speckle photography,³⁸ and

laser speckle flowgraphy³⁹ are not able to clearly distinguish flow in the CNV from the underlying choroidal circulation. A 3D flow imaging technology such as OCT angiography is needed.

Hong et al. used Doppler optical angiography to image CNV associated with neovascular AMD, polypoidal vasculopathy, and myopic macular degeneration.^{25, 26} However, in this pioneering work, it remained difficult to distinguish the CNV from the retinal and choroidal vasculature in the *en face* projection views, and quantification of CNV was not attempted. In this paper, we reported improvements in OCT angiography segmentation, visualization, and quantification to provide comprehensive information that a clinician could use to assess and manage CNV.

Here we investigated the capability of OCT angiography for imaging and quantifying CNV in neovascular AMD patients. A high-speed swept-source OCT system at 1050 nm wavelength provided for deeper penetration compared to standard 830 nm OCT and improved imaging below the RPE. We used a new type of OCT angiography algorithm called SSADA, which is based on detecting the reflectance amplitude (or intensity) variation over time due to flow in vascular volumes. Neither amplitude- nor intensity-based OCT angiography require accurate determination of background tissue phase variation due to motion, and are therefore more robust than Doppler or phase-based OCT angiography.³¹ The SSADA algorithm improves on the standard amplitude or intensity-based algorithms^{20, 22, 23, 40} by enhancing signal and suppressing noise through spectral splitting of the OCT images.²³

We segmented the 3D angiograms into 3 separate vascular layers. Taking advantage of the fact that the outer retinal layer is normally devoid of blood flow, we were able to provide clean *en face* visualization of the CNV structure. By optimizing the choice of color and transparency, we were able to highlight the CNV relative to the inner retinal vascular pattern in a composite *en face* angiogram. Evidence of CNV activity, such as subretinal fluid and intraretinal cysts, was also incorporated into the composite view. This may be very helpful to the clinician in the rapid assessment of CNV and its response to treatment. Since both functional (blood flow) and structural (fluid accumulations) information are taken from a single OCT scan, they are naturally perfectly registered. This is simpler and potentially much faster and robust than combining structural OCT with FA or ICG taken from separate instruments.

Using these new imaging, processing, and display technologies, we successfully identified blood flow in CNVs in five treatment-naïve neovascular AMD cases. The SSADA flow signal was very useful in distinguishing CNV from the surrounding outer retinal tissue, hemorrhage, RPE, BM, and non-flow material under PEDs. Using color OCT cross-sectional angiograms that combined flow and structural information, we were able to determine the position of the CNV relative to the RPE and BM, and thereby classify the CNV as type I, type II, or combined type. In one case, a feeder vessel between the choroid and CNV was successfully visualized (Fig 3), which is rarely possible using FA and ICGA. The position of the CNV on *en face* OCT images was confirmed by FA in all 5 cases. Compared to FA, *en face* OCT angiograms show a more distinct CNV vascular network

pattern that is less obscured by overlying subretinal hemorrhage, as one would expect due to the longer wavelength employed by OCT.

Our pilot study also demonstrated, for the first time, quantitative assessments of CNV area and flow index that is proportional to average avascular density and also flow velocity on the capillary scale. In our small sample of five patients, we noticed higher CNV flow was associated with larger CNV area and type II classification, but larger studies are needed to confirm these associations. Measurements of CNV area and flow index provide new information on CNV activity that may be early indicators of treatment response or relapse. Further studies are needed to assess the clinical utility of these new image-derived metrics.

In addition to providing depth-resolved information of CNV, OCT angiography may provide further insight into choroidal flow and AMD pathogenesis. *En face* choroidal angiograms of the control cases showed confluent signals from choriocapillaris that obscured visualization of larger, deeper choroidal vessels. In all five of the AMD cases, deep choroidal vessels were more apparent and we suspect this is due to loss of choriocapillaris associated with AMD. Some regions of choriocapillaris loss could be attributed to geographic atrophy (Fig. 4F) or due to shadowing from thick hemorrhage, CNV, or PED. However, there were also areas of choriocapillaris loss that could not be attributed to geographic atrophy or shadowing effect. Particularly notable among these areas were focal regions adjacent to CNV where there was total absence of choriocapillaris with loss of both inner and deeper choroidal vessels. We suspect these focal areas of choroidal hypoperfusion with possible outer retinal ischemia may have a role in CNV pathogenesis. Several studies^{41,42} have identified abnormalities in choroidal flow associated with CNV in AMD. McLeod and Luty provided histologic evidence of choriocapillaris atrophy in the vicinity of CNV.⁴³ Although ICGA has often been used to assess the choroidal circulation in CNV, the noninvasive nature of OCT angiography may allow for more frequent assessments of choroidal changes in large, longitudinal clinical studies to identify possible precursors to neovascular AMD development.

Besides its noninvasive nature, OCT angiography has several compelling characteristics that make it a promising modality for clinical use. OCT angiography can be acquired in a few seconds, compared to several minutes for FA. The 3D imaging allows for depth resolution of pathology and separation of individual vascular layers for evaluation. The OCT angiography scan pattern and SSADA processing can be implemented on spectral-domain or swept-source OCT systems without any special hardware modification.

In addition, the new SSADA algorithm allows for a relatively quantitative reliable flow measurements. By using decorrelation instead of variance of reflected signal to measure flow, the measurement is largely independent of OCT signal strength level over a wide range.²⁷ This is important because previous techniques such as the laser Doppler flowmetry (e.g. Heidelberg Retinal Flowmeter) could not reliably compare flow values between individuals due to the effect of signal strength on the measurements.⁴⁴⁻⁴⁸ In SSADA algorithm, background bulk tissue motion was measured and removed at three different levels (see METHODS). This was highly effective as demonstrated by the absence of any retinal flow in normal subjects in the foveal avascular zone and in the outer retina in general. Thus the

flow index is a relatively clean measure of blood flow. Another strength of SSADA is that the decorrelation measures flow in both transverse and axial directions with nearly equal sensitivity. This omnidirectional nature has been verified experimentally.³⁰ This is different from Doppler shift-based techniques,^{13, 14} which is much more sensitive to axial flow than transverse flow. Chorioretinal vessels are largely transverse to the OCT probe beam, but vary over a range of incidence angles. Doppler shift-based flow measurements are biased by incidence angle, unless the Doppler angle is explicitly measured,^{49, 50} or otherwise accounted for.^{51–54} The decorrelation value measured by SSADA is independent of incident angle and therefore a more robust measurement of flow. Certainly, a limitation of decorrelation and its derived flow indexes are that they are in arbitrary units and are affected by imaging parameters such as the time interval between consecutive B-scan (cross-sectional) image frames, split-spectral bandwidth and the wavelength. The spot diameter may also have an effect. However, because these parameters are fixed for OCT systems or could be controlled by software, it is possible to keep these parameters constant and make meaningful measurement that could be compared between individuals and between visits.

There are several limitations to OCT angiography. High scanning speed is needed to provide sufficient cross-sectional frame rate to overcome background eye motion. Therefore the current generation of commercial OCT systems at 20–40 kHz speed may be insufficient. The next generation of OCT systems, running at 70–100 kHz, is likely required. In the present study, the 100 kHz OCT prototype image provided a small 3-mm square field of view. We have recently improved the scan and processing software to provide a 4-mm field of view. However, a larger field of view will require an even higher speed. Because laboratory OCT prototypes of multi-MHz speed have already been reported,^{55–57} we believe the speed and scan size area limitations will be solved as commercial implementation catches up to laboratory technology. FA provides dynamic information currently not available with OCT angiography such as transit time of fluorescein dye to travel to the eye. Additionally, changes in patterns of fluorescence over time (staining, leakage, pooling) are used for identifying and distinguishing various pathological conditions as well as assessment of disease activity, such as CNV. Flow detected on OCT angiography alone will not account for all of this information. However, it is possible in the future that combining information from OCT such as: fluid identified with structural OCT, segmentation of individual structures such as RPE (providing information analogous to staining), and angiographic OCT flow information; may allow for more comprehensive clinical picture with OCT technology.

This pilot study demonstrated the ability of OCT angiography, with the SSADA algorithm, to image CNV and provide quantitative data in its natural state. Additional studies evaluating change in CNV structure, CNV area, and flow index while under treatment with anti-vascular endothelial growth factor therapy are underway. We hope future investigations of quantitative OCT angiography will aid with evaluation and management of neovascular AMD.

Supplementary Material

Refer to Web version on PubMed Central for supplementary material.

Acknowledgments

Support

This work was supported by NIH Grants 1R01 EY023285-01, Rosenbaum's P30EY010572, CTSA grant (UL1TR000128), an unrestricted grant from Research to Prevent Blindness, R01-EY11289-26 and AFOSR FA9550-10-1-0551, German Research Foundation DFG-HO-1791/11-1 and DFG-GSC80-SAOT.

References

1. Eye Diseases Prevalence Research Group. Causes and prevalence of visual impairment among adults in the United States. *Arch Ophthalmol.* 2004; 122:477–85. [PubMed: 15078664]
2. Ferris FL III, Fine SL, Hyman L. Age-related macular degeneration and blindness due to neovascular maculopathy. *Arch Ophthalmol.* 1984; 102:1640–2. [PubMed: 6208888]
3. Ambati J, Ambati BK, Yoo SH, et al. Age-related macular degeneration: etiology, pathogenesis, and therapeutic strategies. *Surv Ophthalmol.* 2003; 48:257–93. [PubMed: 12745003]
4. Stanga PE, Lim JI, Hamilton P. Indocyanine green angiography in chorioretinal diseases: indications and interpretation: an evidence-based update. *Ophthalmology.* 2003; 110:15–21. [PubMed: 12511340]
5. Lopez-Saez MP, Ordoqui E, Tornero P, et al. Fluorescein-induced allergic reaction. *Ann Allergy Asthma Immunol.* 1998; 81:428–30. [PubMed: 9860035]
6. Huang D, Swanson EA, Lin CP, et al. Optical coherence tomography. *Science.* 1991; 254:1178–81. [PubMed: 1957169]
7. Hee MR, Bauman CR, Puliafito CA, et al. Optical coherence tomography of age-related macular degeneration and choroidal neovascularization. *Ophthalmology.* 1996; 103:1260–70. [PubMed: 8764797]
8. Do DV, Gower EW, Cassard SD, et al. Detection of new-onset choroidal neovascularization using optical coherence tomography: the AMD DOC Study. *Ophthalmology.* 2012; 119:771–8. [PubMed: 22297028]
9. Coscas F, Coscas G, Souied E, et al. Optical coherence tomography identification of occult choroidal neovascularization in age-related macular degeneration. *Am J Ophthalmol.* 2007; 144:592–9. [PubMed: 17698019]
10. Framme C, Panagakos G, Birngruber R. Effects on choroidal neovascularization after anti-VEGF upload using intravitreal ranibizumab, as determined by spectral domain-optical coherence tomography. *Invest Ophthalmol Vis Sci.* 2010; 51:1671–6. [PubMed: 19875667]
11. Sayanagi K, Sharma S, Yamamoto T, Kaiser PK. Comparison of spectral-domain versus time-domain optical coherence tomography in management of age-related macular degeneration with ranibizumab. *Ophthalmology.* 2009; 116:947–55. [PubMed: 19232732]
12. de Bruin DM, Burnes DL, Loewenstein J, et al. In vivo three-dimensional imaging of neovascular age-related macular degeneration using optical frequency domain imaging at 1050 nm. *Invest Ophthalmol Vis Sci.* 2008; 49:4545–52. [PubMed: 18390638]
13. Hong YJ, Makita S, Jaillon F, et al. High-penetration swept source Doppler optical coherence angiography by fully numerical phase stabilization. *Opt Express* [serial online]. 2012; 20:2740–60. Available at: <http://www.opticsinfobase.org/oe/fulltext.cfm?uri=oe-20-3-2740&id=226741>.
14. Grulkowski I, Gorczynska I, Szkulmowski M, et al. Scanning protocols dedicated to smart velocity ranging in spectral OCT. *Opt Express* [serial online]. 2009; 17:23736–54. Available at: <http://www.opticsinfobase.org/oe/abstract.cfm?uri=oe-17-26-23736>.
15. Liu G, Qi W, Yu L, Chen Z. Real-time bulk-motion-correction free Doppler variance optical coherence tomography for choroidal capillary vasculature imaging. *Opt Express* [serial online]. 2011; 19:3657–66. Available at: <http://www.opticsinfobase.org/oe/fulltext.cfm?uri=oe-19-4-3657&id=210023>.
16. Wang L, Wang Y, Guo S, et al. Frequency domain phase-resolved optical Doppler and Doppler variance tomography. *Opt Commun.* 2004; 242:345–50.

17. Yu L, Chen Z. Doppler variance imaging for three-dimensional retina and choroid angiography. *J Biomed Opt.* 2010; 15:016029. [PubMed: 20210473]
18. Fingler J, Zawadzki RJ, Werner JS, et al. Volumetric microvascular imaging of human retina using optical coherence tomography with a novel motion contrast technique. *Opt Express* [serial online]. 2009; 17:22190–200. Available at: <http://www.opticsinfobase.org/oe/abstract.cfm?uri=oe-17-24-22190>.
19. Kim DY, Fingler J, Werner JS, et al. In vivo volumetric imaging of human retinal circulation with phase-variance optical coherence tomography. *Biomed Opt Express* [serial online]. 2011; 2:1504–13. Available at: <http://www.opticsinfobase.org/boe/fulltext.cfm?uri=boe-2-6-1504&id=213832>.
20. Hendargo HC, Estrada R, Chiu SJ, et al. Automated non-rigid registration and mosaicing for robust imaging of distinct retinal capillary beds using speckle variance optical coherence tomography. *Biomed Opt Express* [serial online]. 2013; 4:803–21. Available at: <http://www.opticsinfobase.org/boe/fulltext.cfm?uri=boe-4-6-803&id=253337>.
21. Mariampillai A, Leung MK, Jarvi M, et al. Optimized speckle variance OCT imaging of microvasculature. *Opt Lett.* 2010; 35:1257–9. [PubMed: 20410985]
22. Mariampillai A, Standish BA, Moriyama EH, et al. Speckle variance detection of microvasculature using swept-source optical coherence tomography. *Opt Lett.* 2008; 33:1530–2. [PubMed: 18594688]
23. Enfield J, Jonathan E, Leahy M. In vivo imaging of the microcirculation of the volar forearm using correlation mapping optical coherence tomography (cmOCT). *Biomed Opt Express* [serial online]. 2011; 2:1184–93. Available at: <http://www.opticsinfobase.org/boe/fulltext.cfm?uri=boe-2-5-1184&id=211771>.
24. Jonathan E, Enfield J, Leahy MJ. Correlation mapping method for generating microcirculation morphology from optical coherence tomography (OCT) intensity images. *J Biophotonics.* 2011; 4:583–7. [PubMed: 21887769]
25. Miura M, Makita S, Iwasaki T, Yasuno Y. Three-dimensional visualization of ocular vascular pathology by optical coherence angiography in vivo. *Invest Ophthalmol Vis Sci.* 2011; 52:2689–95. [PubMed: 21273541]
26. Hong YJ, Miura M, Makita S, et al. Noninvasive investigation of deep vascular pathologies of exudative macular diseases by high-penetration optical coherence angiography. *Invest Ophthalmol Vis Sci.* 2013; 54:3621–31. [PubMed: 23633664]
27. Jia Y, Morrison JC, Tokayer J, et al. Quantitative OCT angiography of optic nerve head blood flow. *Biomed Opt Express* [serial online]. 2012; 3:3127–37. Available at: <http://www.opticsinfobase.org/boe/fulltext.cfm?uri=boe-3-12-3127&id=245369>.
28. American National Standard for Safe Use of Lasers, ANSI Z136.1–2007. Orlando, FL: Laser Institute of America; 2007.
29. Barton J, Stromski S. Flow measurement without phase information in optical coherence tomography images. *Opt Express* [serial online]. 2005; 13:5234–9. Available at: <http://www.opticsinfobase.org/oe/abstract.cfm?uri=oe-13-14-5234>.
30. Tokayer J, Jia Y, Dhalla AH, Huang D. Blood flow velocity quantification using split-spectrum amplitude-decorrelation angiography with optical coherence tomography. *Biomed Opt Express* [serial online]. 2013; 4:1909–24. Available at: <http://www.opticsinfobase.org/boe/fulltext.cfm?uri=boe-4-10-1909&id=260835>.
31. Liu G, Lin AJ, Tromberg BJ, Chen Z. A comparison of Doppler optical coherence tomography methods. *Biomed Opt Express* [serial online]. 2012; 3:2669–80. Available at: <http://www.opticsinfobase.org/boe/fulltext.cfm?uri=boe-3-10-2669&id=242508>.
32. Kraus MF, Potsaid B, Mayer MA, et al. Motion correction in optical coherence tomography volumes on a per A-scan basis using orthogonal scan patterns. *Biomed Opt Express* [serial online]. 2012; 3:1182–99. Available at: <http://www.opticsinfobase.org/boe/fulltext.cfm?uri=boe-3-6-1182&id=233031>.
33. Tan O, Chopra V, Lu AT, et al. Detection of macular ganglion cell loss in glaucoma by Fourier-domain optical coherence tomography. *Ophthalmology.* 2009; 116:2305–14. [PubMed: 19744726]
34. Tan O, Li G, Lu AT, et al. Mapping of macular substructures with optical coherence tomography for glaucoma diagnosis. *Ophthalmology.* 2008; 115:949–56. [PubMed: 17981334]

35. Chan TF, Vese LA. Active contours without edges. *IEEE Trans Image Process.* 2001; 10:266–77. [PubMed: 18249617]
36. Giovannini A, Amato GP, Mariotti C, Scassellati-Sforzolini B. OCT imaging of choroidal neovascularisation and its role in the determination of patients' eligibility for surgery. *Br J Ophthalmol.* 1999; 83:438–42. [PubMed: 10434866]
37. Michelson G, Schmauss B, Langhans MJ, et al. Principle, validity, and reliability of scanning laser Doppler flowmetry. *J Glaucoma.* 1996; 5:99–105. [PubMed: 8795741]
38. Briers JD, Fercher AF. Retinal blood-flow visualization by means of laser speckle photography. *Invest Ophthalmol Vis Sci.* 1982; 22:255–9. [PubMed: 7056639]
39. Tamaki Y, Araie M, Kawamoto E, et al. Noncontact, two-dimensional measurement of retinal microcirculation using laser speckle phenomenon. *Invest Ophthalmol Vis Sci.* 1994; 35:3825–34. [PubMed: 7928179]
40. Motaghianezam R, Fraser S. Logarithmic intensity and speckle-based motion contrast methods for human retinal vasculature visualization using swept source optical coherence tomography. *Biomed Opt Express* [serial online]. 2012; 3:503–21. Available at: <http://www.opticsinfobase.org/boe/fulltext.cfm?uri=boe-3-3-503&id=227627>.
41. Hayashi K, de Laey JJ. Indocyanine green angiography of choroidal neovascular membranes. *Ophthalmologica.* 1985; 190:30–9. [PubMed: 2578633]
42. Melrose MA, Magargal LE, Goldberg RE, Annesley WH Jr. Subretinal neovascular membranes associated with choroidal nonperfusion and retinal ischemia. *Ann ophthalmol.* 1987; 19:396–9. [PubMed: 2446561]
43. McLeod DS, Grebe R, Bhutto I, et al. Relationship between RPE and choriocapillaris in age-related macular degeneration. *Invest Ophthalmol Vis Sci.* 2009; 50:4982–91. [PubMed: 19357355]
44. Petrig, BL.; Riva, CE. Optic nerve head laser Doppler flowmetry: principles and computer analysis. In: Kaiser, HJ.; Flammer, J.; Hendrickson, P., editors. *Ocular Blood Flow: New Insights into the Pathogenesis of Ocular Diseases.* Basel, Switzerland: Karger; 1995. p. 120-7.
45. Petrig BL, Riva CE, Hayreh SS. Laser Doppler flowmetry and optic nerve head blood flow. *Am J Ophthalmol.* 1999; 127:413–25. [PubMed: 10218694]
46. Riva CE. Basic principles of laser Doppler flowmetry and application to the ocular circulation. *Int Ophthalmol.* 2001; 23:183–9. [PubMed: 11944839]
47. Jonescu-Cuypers CP, Chung HS, Kagemann L, et al. New neuroretinal rim blood flow evaluation method combining Heidelberg retina flowmetry and tomography. *Br J Ophthalmol.* 2001; 85:304–9. [PubMed: 11222335]
48. Obeid A, Barnett N, Dougherty G, Ward G. A critical review of laser Doppler flowmetry. *J Med Eng Technol.* 1990; 14:178–81. [PubMed: 2231661]
49. Wang Y, Bower BA, Izatt JA, et al. Retinal blood flow measurement by circumpapillary Fourier domain Doppler optical coherence tomography. *J Biomed Opt.* 2008; 13:064003. [PubMed: 19123650]
50. Wang Y, Fawzi AA, Varma R, et al. Pilot study of optical coherence tomography measurement of retinal blood flow in retinal and optic nerve diseases. *Invest Ophthalmol Vis Sci.* 2011; 52:840–5. [PubMed: 21051715]
51. Pedersen CJ, Huang D, Shure MA, Rollins AM. Measurement of absolute flow velocity vector using dual-angle, delay-encoded Doppler optical coherence tomography. *Opt Lett.* 2007; 32:506–8. [PubMed: 17392903]
52. Srinivasan VJ, Sakadzic S, Gorczynska I, et al. Quantitative cerebral blood flow with optical coherence tomography. *Opt Express* [serial online]. 2010; 18:2477–94. Available at: <http://www.opticsinfobase.org/oe/abstract.cfm?uri=oe-18-3-2477>.
53. Baumann B, Potsaid B, Kraus MF, et al. Total retinal blood flow measurement with ultrahigh speed swept source/Fourier domain OCT. *Biomed Opt Express* [serial online]. 2011; 2:1539–52. Available at: <http://www.opticsinfobase.org/boe/fulltext.cfm?uri=boe-2-6-1539&id=213997>.
54. Zhi Z, Yin X, Dziennis S, et al. Optical microangiography of retina and choroid and measurement of total retinal blood flow in mice. *Biomed Opt Express* [serial online]. 2012; 3:2976–86. Available at: <http://www.opticsinfobase.org/boe/fulltext.cfm?uri=boe-3-11-2976&id=244697>.

55. Choi DH, Hiro-Oka H, Shimizu K, Ohbayashi K. Spectral domain optical coherence tomography of multi-MHz A-scan rates at 1310 nm range and real-time 4D-display up to 41 volumes/second. *Biomed Opt Express* [serial online]. 2012; 3:3067–86. Available at: <http://www.opticsinfobase.org/boe/fulltext.cfm?uri=boe-3-12-3067&id=244867>.
56. Klein, T.; Wieser, W.; André, R., et al. In: Izatt, JA.; Fujimoto, JG.; Tuchin, VV., editors. Multi-MHz FDML OCT: snapshot retinal imaging at 6.7 million axial-scans per second; Proc SPIE 8213: Optical Coherence Tomography and Coherence Domain Optical Methods in Biomedicine XVI; San Francisco, CA: SPIE; 2012. p. 82131E
57. Potsaid, B.; Jayaraman, V.; Fujimoto, JG., et al. In: Izatt, JA.; Fujimoto, JG.; Tuchin, VV., editors. MEMS tunable VCSEL light source for ultrahigh speed 60kHz–1MHz axial scan rate and long range centimeter class OCT imaging; Proc. SPIE 8213: Optical Coherence Tomography and Coherence Domain Optical Methods in Biomedicine XVI; San Francisco, CA: SPIE; 2012. p. 82130M

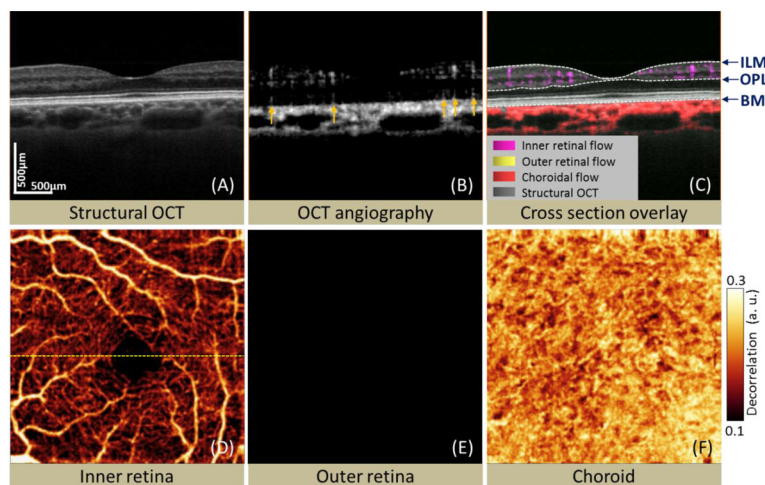


Figure 1. Healthy control case. (A) Cross-sectional optical coherence tomography (OCT) reflectance image (conventional OCT B-scan). (B) Cross-sectional OCT angiography. Arrows point to locations where flows in inner retinal vessels are projected onto bright photoreceptor and retinal pigment epithelium layers. (C) Cross-sectional color OCT angiogram. The internal limiting membrane (ILM) and outer plexiform layer (OPL) and Bruch's membrane (BM) are the boundaries separating inner retinal, outer retinal, and choroidal circulations. (D) *En face* angiogram of the inner retina. The dashed line indicates the cross-sections shown in A–C above. (E) *En face* angiogram of the outer retina. (F) *En face* angiogram of the choroid. *En face* angiograms were produced by maximum flow projections within segmented layers and span a 3×3 mm area. Higher decorrelation value corresponds to higher blood flow velocity.

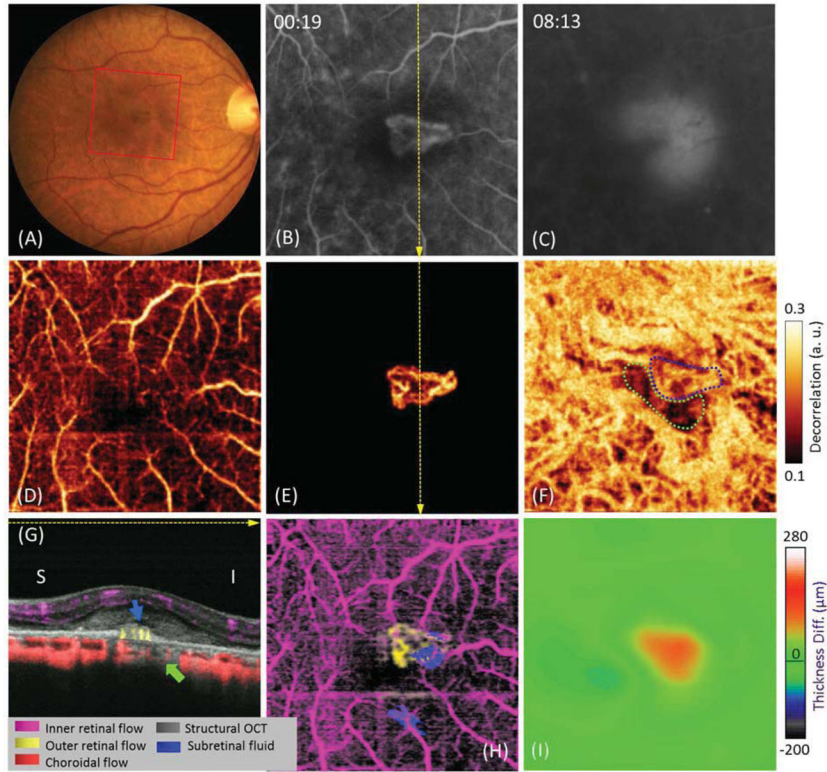


Figure 2. Age-related macular degeneration case 1: type I choroidal neovascularization (CNV). (A) Color fundus photograph showing subretinal hemorrhage. Red square outlines the area shown on angiograms below. (B) Early phase fluorescein angiogram (FA). (C) Late phase FA. (D) *En face* optical coherence tomography (OCT) angiogram of the inner retina. (E) *En face* angiogram of the outer retina showing the CNV. The yellow dashed lines indicate the position of OCT cross-section shown in Panel G. Yellow arrows indicate the superior to inferior direction. (F) *En face* angiogram of the choroid showing patchy flow directly under the CNV (blue dotted outline) and an adjacent area of reduced flow (green dotted outline). (G) Cross-sectional color OCT angiogram showing the CNV (yellow) was predominantly under the retinal pigment epithelium (RPE). The blue arrow shows the location of the subretinal fluid. The green arrow corresponds to the green dashed outline in Panel F showing a focal region of reduced choroidal flow adjacent to the CNV. S: superior; I: inferior. (H) Composite *en face* OCT angiograms showing most subretinal fluid (dark blue) inferior to the CNV. (I) Retinal thickness deviation map showing retinal thickening over the CNV.

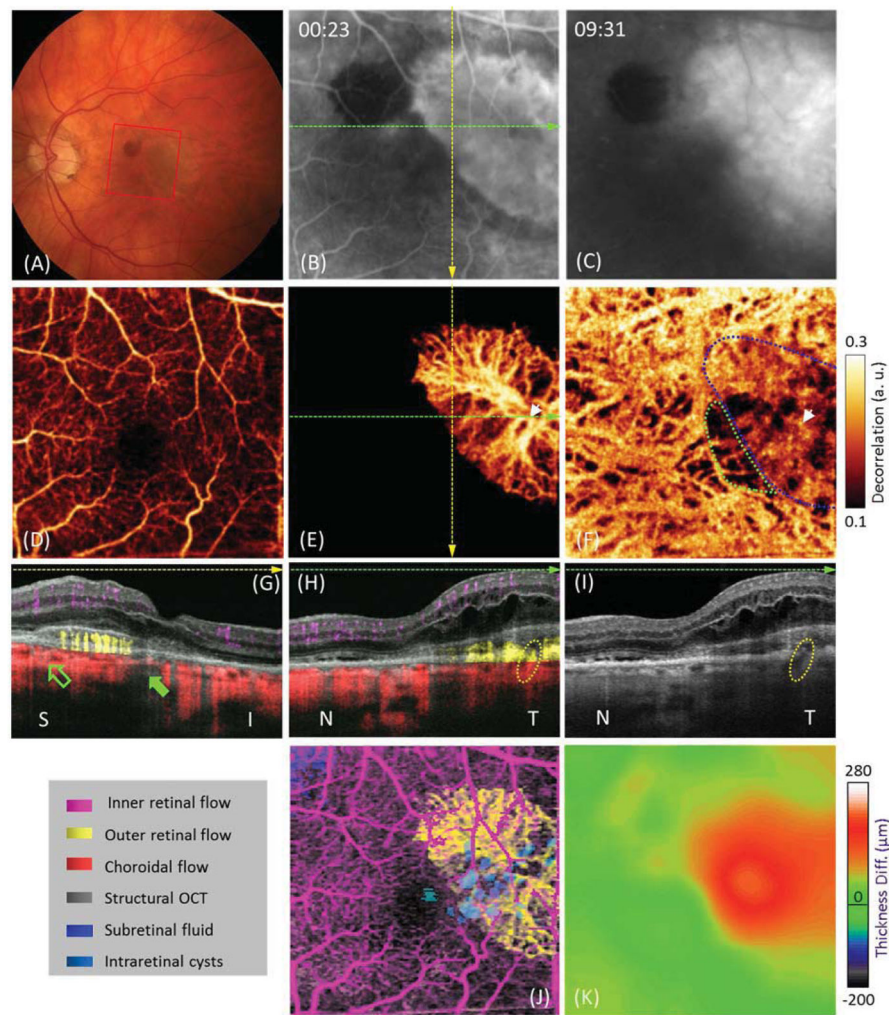


Figure 3. Age-related macular degeneration case 2: type II choroidal neovascularization (CNV). (A) Fundus photography showing subretinal hemorrhage. The red square outlines the area shown on angiograms below. (B) Early phase fluorescein angiogram (FA). (C) Late phase FA. (D) *En face* optical coherence tomography (OCT) angiogram of the inner retina. (E) *En face* OCT angiogram of the outer retina showing the CNV. The yellow and green dashed lines indicate the position of OCT cross-section shown in Panels G, H and I. (F) *En face* angiogram of the choroid showing the patchy reduced flow directly under the CNV (blue dotted outline) and an adjacent area of reduced flow (green dotted outline). (G) Vertical cross-sectional color OCT angiogram showing the CNV (yellow) was predominantly above the retinal pigment epithelium (RPE). The green solid arrow corresponds to the green dotted outline in F showing a focal region of reduced choroidal flow inferonasal to the CNV. The green hollow arrow points out a high choroidal flow signal superior to the CNV. (H) Horizontal cross-sectional color OCT angiogram showing the feeder vessel (yellow dotted circle) that corresponds to the white arrows in Panels E and F. Also note cystic intraretinal fluid above the CNV. (I) Horizontal cross-sectional OCT reflectance image showing the feeder vessel seen as a flow void. (J) Composite *en face* OCT angiogram showing subretinal

fluid (dark blue) at the superonasal corner and intraretinal fluid (light blue) over the CNV. (K) Retinal thickness deviation map showing thickening over the CNV. Fly through movies of 3D color OCT angiograms are available as a supplement (Video 1 and 2).

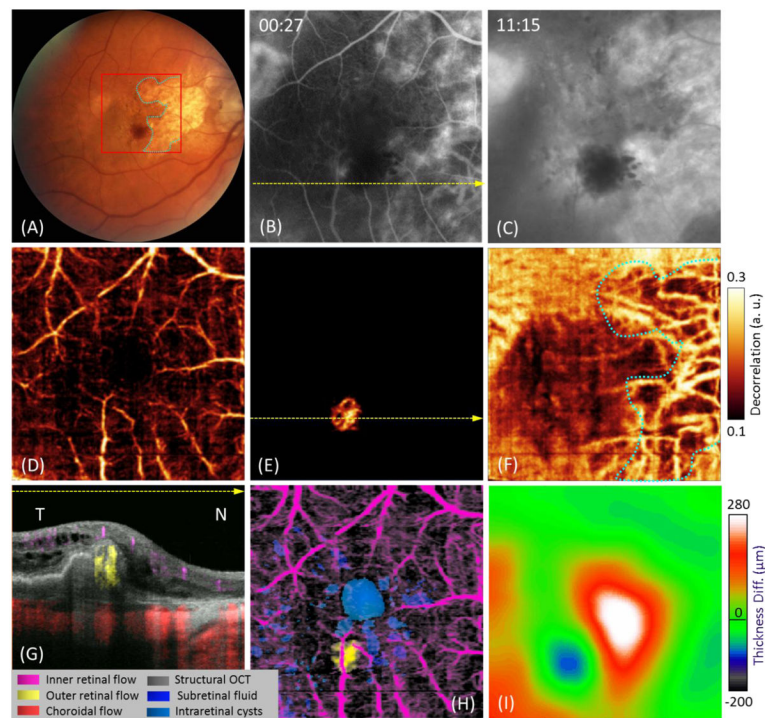


Figure 4.

Age-related macular degeneration case 3: combined type I and type II choroidal neovascularization (CNV). (A) Fundus photography showing subretinal hemorrhage, retinal pigment epithelium (RPE) tear, and geographic atrophy (blue dashed outline). Red square outlines area shown on angiograms below. (B) Early phase fluorescein angiogram (FA). (C) Late phase FA. (D) *En face* optical coherence tomography (OCT) angiogram of the inner retina. (E) *En face* angiograms of the outer retina showing the CNV. The yellow dashed lines indicate the position of OCT cross-section shown in Panel G. (F) *En face* angiogram of the choroid showing diffuse reduction of flow signal under the pigment epithelial detachment and choriocapillaris defect in the area of geographic atrophy (blue dashed outline). (G) Cross-sectional color OCT angiogram showing the CNV both above and below the RPE. The subretinal hemorrhage was over the CNV and overshadowed the CNV at its nasal edge. (H) Composite *en face* OCT angiograms. (I) Retinal thickness deviation map showing thinning over the CNV and thickening around it.

Table 1

Summary of CNV types, CNV area and CNV flow index of five scanned AMD cases

AMD Case #	Sex/Age	CNV Types	CNV Area (mm ²)	CNV Flow Index (a.u.)
1	F/65	type I	0.29	0.127
2	F/76	type II	2.18	0.146
3	F/88	combined	0.13	0.130
4	F/85	type II	0.89	0.148
5	M/70	combined	0.05	0.120

AMD: Age-related macular degeneration; CNV: Choroidal neovascularization; F: Female; M: Male; a.u.: arbitrary unit